Quantum phase diagram of spin-1 J_1-J_2 Heisenberg model on the square lattice: An infinite projected entangled-pair state and density matrix renormalization group study

R. Haghshenas,[1,*] Wang-Wei Lan,[2] Shou-Shu Gong,[3,†] and D. N. Sheng[1]
[1]*Department of Physics and Astronomy, California State University, Northridge, California 91330, USA*
[2]*Département de Physique and Institut Quantique, Université de Sherbrooke, Québec, Canada J1K 2R1*
[3]*Department of Physics, Beihang University, Beijing 100191, China*

(Received 13 February 2018; revised manuscript received 27 April 2018; published 31 May 2018)

We study the spin-1 Heisenberg model on the square lattice with the antiferromagnetic nearest-neighbor J_1 and the next-nearest-neighbor J_2 couplings by using the infinite projected entangled-pair state (iPEPS) ansatz and the density matrix renormalization group (DMRG) calculation. The iPEPS simulation, which studies the model directly in the thermodynamic limit, finds a crossing of the ground state from the Néel magnetic state to the stripe magnetic state at $J_2/J_1 \simeq 0.549$, showing a direct phase transition. In the finite-size DMRG calculation on the cylinder geometry up to the cylinder width $L_y = 10$, we find that around the same critical point the Néel and the stripe orders are strongly suppressed, which implies the absence of an intermediate phase. Both calculations identify that the stripe order comes with a first-order transition at $J_2/J_1 \simeq 0.549$. Our results indicate that unlike the spin-1/2 J_1-J_2 square model, quantum fluctuations in the spin-1 model may not be strong enough to stabilize an intermediate nonmagnetic phase.

DOI: 10.1103/PhysRevB.97.184436

I. INTRODUCTION

Frustrated magnetic systems play a key role in understanding the exotic phases of matter [1,2]. As we know, frustration can enhance quantum fluctuations by imposing incompatibility on the local interaction energy to be simultaneously satisfied, which may destroy magnetic long-range order and lead the systems into novel quantum phases, such as valence-bond solid (VBS) [3–5] and quantum spin liquid [6–8]. In addition, quantum phase transitions between such phases may defy the Ginzburg-Landau theory—referred to as the deconfined quantum criticality [9]—which makes the physics of frustrated quantum magnetism a fascinating subject in both theoretical and experimental senses. Among the various frustrated antiferromagnets, the spin-S J_1-J_2 square Heisenberg models [10–13] are well-known examples and have stimulated extensive theoretical studies over the past two decades. The competing interactions in such systems may stabilize a nonmagnetic intermediate phase if quantum fluctuations are not strongly suppressed [10–13]. One of the successful examples is the spin-1/2 J_1-J_2 model, in which a nonmagnetic intermediate phase has been identified by using different methods although the nature of the phase is still controversial [14–20].

Meanwhile, the frustrated spin-1 square Heisenberg models (SHMs) are also typical for studying frustrated magnetism. Recently, studies on the magnetism of iron-based superconductors have drawn extensive interest in investigating novel quantum phases, particularly the nonmagnetic phase with lattice nematic order, in different spin-1 SHMs [21–33]. Among the various models, the spin-1 J_1-J_2 SHM is probably the most fundamental model, which is defined as

$$H = J_1 \sum_{\langle i,j \rangle} \mathbf{S}_i \cdot \mathbf{S}_j + J_2 \sum_{\langle\langle i,j \rangle\rangle} \mathbf{S}_i \cdot \mathbf{S}_j,$$

where $\langle i,j \rangle$ and $\langle\langle i,j \rangle\rangle$ denote the nearest-neighbor and the next-nearest-neighbor pairs, and J_1 and J_2 are both antiferromagnetic (AFM) couplings. We set $J_1 = 1$ as the energy scale. Classically, this model in the large-S limit has a Néel and a stripe AFM phase separated at $J_2 = 0.5$. After considering quantum fluctuations, the early studies based on the modified spin-wave theory [12,34] and the Schwinger-Boson mean-field theory [35] predicted that quantum fluctuations for the systems with spin magnitude $S > 0.7$ are not strong enough to stabilize a nonmagnetic intermediate phase. Thus, mean-field results suggested a direct phase transition from the Néel to the stripe AFM phase for the spin-1 model. This result was later confirmed by the coupled cluster method, which found a first-order transition between the Néel and the stripe phase at $J_2 \simeq 0.55$ [36]. Interestingly, the recent density matrix renormalization group (DMRG) study [37] challenged this result: it predicted a nonmagnetic phase in the small intermediate region for $0.525 \lesssim J_2 \lesssim 0.555$ and suggested that this nonmagnetic phase might be continuously connected to the limit of the decoupled Haldane spin chains [38] by tuning the spacial anisotropic couplings J_{1x} and J_{1y}. Such a nonmagnetic phase in a spin-1 model is quite interesting not only because it goes beyond the physics in the mean-field description but also because it might be related to the nematic nonmagnetic phase in the iron-based superconductor material FeSe [26].

In this article, our main goal is to reexamine the phase diagram of the spin-1 J_1-J_2 SHM based on the variational tensor-network ansatz and the DMRG simulation [39]. In previous studies, while the mean-field calculation may not

*reza.haghshenas@csun.edu
†shoushu.gong@buaa.edu.cn

fully consider quantum fluctuations [12,34,35], use of the DMRG simulation may result in difficulty in pinning down the intermediate region as a nonmagnetic phase due to the finite-size effects [37]. To this end, we use state-of-the-art numerical methods to systematically study the model. We use the U(1)-symmetric infinite projected entangled-pair state (iPEPS) ansatz [40,41] and the SU(2)-symmetric finite-size DMRG to study the system from different limits: the iPEPS is directly applied in the thermodynamic limit, significantly diminishing possible finite-size effects; SU(2)-symmetric DMRG obtains accurate results in a finite-size system. In the iPEPS ansatz, the only control parameter is the so-called bond dimension D which controls entanglement in the system. To simulate highly entangled states (larger bond dimensions), we implement U(1) symmetry into the iPEPS ansatz [42]. We expect that a close comparison of these different approaches could substantially improve our understanding of the intermediate regime.

In our iPEPS simulation, we use a hysteresis effect to accurately determine the quantum phase transition and its nature [43]. We initialize the iPEPS ansatz with different types of wave functions to find the lowest variational ground-state energy. It is found that either the Néel or the stripe state provides the lowest iPEPS energy throughout the coupling parameter range. The energies of the Néel and the stripe states cross each other at the critical point $J_2 \simeq 0.549$, where the magnetic order parameters (defined later) remain nonzero in the $D \to \infty$ limit, suggesting a first-order phase transition between the two magnetic order phases. We also observe that the correlation length is unlikely to show a divergent behavior around the transition point, further supporting a first-order transition. In our DMRG calculation with the improved system size for size-scaling analysis, we find that the Néel order could persist to $J_2 \simeq 0.545$ and the stripe order increases sharply at $J_2 \simeq 0.55$, showing a very narrow nonmagnetic regime, which is quite smaller than the previous DMRG result of $\sim$0.03 [37]. The fast-shrinking intermediate regime, which is observed in the finite-size scaling with increased system size in the DMRG results, may suggest the vanishing nonmagnetic phase. The nonmagnetic phase with a strong lattice nematicity in spin-1 models, which has been proposed for the nematic paramagnetic phase of FeSe [26], might be stabilized by considering other competing and/or frustrating interactions.

The paper is organized as follows. We briefly discuss the numerical methods and define the order parameters used in this paper in Sec. II. Our main numerical results are presented in Sec. III. In Sec. III A, we compare the variational ground-state energy obtained by the numerical methods and discuss the iPEPS results by studying the variational energy of competitive ordered states and the behavior of the spin correlation length. In Sec. III B, we provide a systematic study of the nematic and magnetic order parameters and also discuss the behavior of the gap by using DMRG. Finally, we summarize our findings in Sec. IV.

II. METHODS

A. iPEPS anstaz

The iPEPS ansatz provides an efficient variational method to approximate the ground-state wave functions of the two-dimensional spin systems in the thermodynamic limit [44]. The iPEPS is made of some building-block tensors which are periodically repeated through the infinite two-dimensional (2D) lattice. The tensors are connected to each other by the so-called virtual bonds to construct a geometrical pattern (usually) similar to the 2D lattice. The main idea is to variationally minimize the expectation value of energy with respect to the tensors (variational parameters) to eventually obtain an approximation of the ground state. The bond dimension of the virtual bonds denoted by D determines the number of variational parameters, hence controlling the accuracy of the iPEPS ansatz. It also represents the amount of entanglement, so that by increasing it even "highly entangled states" can be accurately approximated [45].

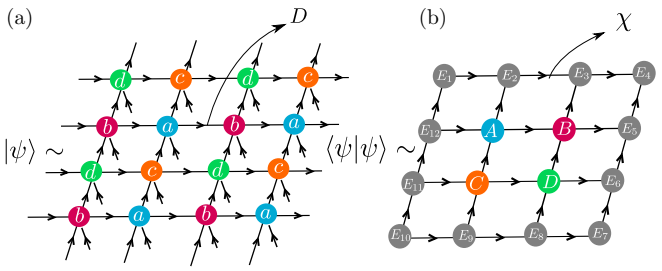

FIG. 1. Tensor-network representation of a U(1)-symmetric iPEPS $|\psi\rangle$. (a) The iPEPS $|\psi\rangle$ is made of the U(1)-invariant tensors $\{a,b,c,d\}$ periodically repeated through the infinite square lattice. (b) The scalar product $\langle\psi|\psi\rangle$ is calculated by using the so-called environment tensors $\{E_1,\ldots,E_{12}\}$ obtained by the corner transfer matrix renormalization group approach. The bond dimensions D and χ control the accuracy of the iPEPS anstaz.

In this paper, as shown in Fig. 1(a), we use (up to) a 2×2 unit cell iPEPS constructed from five-rank independent tensors $\{a,b,c,d\}$. We exploit U(1) symmetry, making all tensors $\{a,b,c,d\}$ be U(1) invariant, to reach the larger bond dimensions up to $D \sim 9$ [46]. We perform the optimization procedure by using imaginary-time evolution in the class of the iPEPS [47]

$$|\psi_{i+1}\rangle = e^{-\tau H}|\psi_i\rangle,$$

where $|\psi_{i+1}\rangle$ at each step i is represented by an iPEPS—τ stands for imaginary time. A first-order Trotter-Suzuki decomposition [48] is used to efficiently represent the imaginary time-evolution operator $e^{-\tau H}$. We also use the so-called full-update scheme [20,49] to truncate the bond dimension: at each step, an imaginary time-evolution operator increases the bond dimension of virtual bonds, so a truncation procedure is needed to prevent the exponential growth of the parameters. In the case of the spin-1 J_1-J_2 SHM, we find that the computationally cheaper scheme, i.e., the simple update [50–52], does not give us accurate results, but its output could be used as a good initial state for the full-update scheme.

A corner transfer matrix renormalization group (CTMRG) approach [53–55] is used to evaluate the expectation values of observables and also to obtain the so-called environment tensors (needed within the optimization procedure). The accuracy of the CTMRG approach is controlled by the "boundary" bond dimension of the environment tensors denoted by χ [see Fig. 1(b)]. We always take χ large enough to

diminish the error due to the environment approximation: for the largest bond dimension $D = 9$, it approximately requires $\chi \sim 100$ to make the relative error of the ground-state energy negligible.

In order to recognize magnetically ordered phases, we calculate the magnetic order parameter defined by

$$m = \tfrac{1}{4}(|\langle \mathbf{S}_a \rangle| + |\langle \mathbf{S}_b \rangle| + |\langle \mathbf{S}_c \rangle| + |\langle \mathbf{S}_d \rangle|),$$

where operator $\mathbf{S}_a$ is acting on tensor a (analogous for other operators). Since the magnetically ordered states break the SU(2) symmetry, so we expect to obtain a nonzero value of m in the $D \to \infty$ limit.

In addition, we use the texture of the local bond J_1 energy to detect the lattice symmetry breaking, as defined by $\Delta T_{x(y)} = \max(E_{x(y)}) - \min(E_{x(y)})$ and $\Delta T_{x-y} = \max(E_y) - \min(E_x)$. The order of taking the maximum and the minimum is chosen to enlarge the order parameters; although it does not significantly affect the results. The symbols E_x and E_y stand for the local bond energy in the unit cell for the horizontal and vertical directions—note that for each virtual bond we might obtain a different value of $E_{x,y}$. The order parameters ΔT_{x-y} and ΔT_x respectively detect rotational and translational lattice symmetry breaking. Similarly, a finite value of $\Delta T_{x-y,x}$ in the $D \to \infty$ limit implies a lattice symmetry breaking. By using the order parameters $\{m, \Delta T_{x-y,x}\}$, we could distinguish between different types of ordered states, such as Néel, stripe, VBS, and Haldane.

In order to estimate the variational energy and the order parameters, we use a polynomial and a linear fit with bond dimension $1/D$, respectively. Our intuition to using such extrapolations is that it provides an accurate estimation of these quantities at point $J_2 = 0$. The results could be compared to those of a quantum Monte Carlo method [56], as at this point there is no sign problem. For example, the relative error of our estimation of the magnetic order parameter is of the order $\Delta m = \frac{m_{D\to\infty} - m_{\mathrm{MC}}}{m_{\mathrm{MC}}} < 10^{-2}$ (see also Ref. [32] for similar results).

Finally, we utilize the spin-spin correlation function $C^s(r)$ and the corresponding correlation length ξ^s to distinguish a quantum critical point (phase) from the ordered phases. They are defined by

$$C^s(r) = \langle \mathbf{S}_{(x,y)} \cdot \mathbf{S}_{(x+r,y)} \rangle - \langle \mathbf{S}_{(x,y)} \rangle^2,$$

$$\log[C^s(r)] = \left(\frac{-1}{\xi^s}\right) r + \text{const } r \gg 1.$$

Usually, a finite bond dimension D (usually) induces a finite correlation length [57,58], thus, to determine the true nature of the phases, we need to study the correlation length in the large-D limit. For a quantum critical point, by increasing D, one expects the correlation length to grow rapidly. On the other hand, for the ordered phases such as the Néel phase, it tends to a finite value in the large-D limit.

B. DMRG method

We implement the DMRG method [59] for studying a finite-size system. A rectangular cylinder (RC) geometry is used in our calculation, which has the periodic boundary conditions in the y direction and the open boundary conditions in the x direction. We denote the cylinder as RCL_y-L_x, where L_y and L_x are the numbers of sites along the y direction and the x direction, respectively. In order to obtain accurate results on a wide cylinder with L_y up to 10, we use an SU(2)-symmetric DMRG [60] by keeping as many as about 20 000 U(1)-equivalent states (6000 SU(2) optimal states). The truncation error is less than 1×10^{-5}.

In order to detect the magnetic orders, we calculate the magnetic order parameter $m^2(\mathbf{q}) = \frac{1}{N_s^2} \sum_{i,j} \langle \mathbf{S}_i \cdot \mathbf{S}_j \rangle e^{i\mathbf{q}\cdot(\mathbf{r}_i - \mathbf{r}_j)}$, where N_s is the summed total site number. For the Néel and the stripe AFM order, the order parameter $m^2(\mathbf{q})$ shows the peaks at $\mathbf{q} = (\pi,\pi)$ and $\mathbf{q} = (0,\pi)/(\pi,0)$, which are denoted as $m^2(\pi,\pi)$ and $m^2(0,\pi)/(\pi,0)$. For the stripe order, since our cylinder geometry breaks the lattice symmetry, the DMRG calculation selects the momentum at $\mathbf{q} = (0,\pi)$. To obtain the order parameters with reduced boundary effects, we use the spin correlation functions of the middle $L_y \times L_y$ sites on the RCL_y-$2L_y$ cylinder.

We also define the bond nematic order σ_1 as the difference between the horizontal and vertical J_1 bond energy, namely, $\sigma_1 = \langle \mathbf{S}_i \cdot \mathbf{S}_{i+\hat{x}} \rangle - \langle \mathbf{S}_i \cdot \mathbf{S}_{i+\hat{y}} \rangle$ (i could be any lattice site in the bulk of the cylinder like the translational symmetry shown below; $\hat{x}$ and $\hat{y}$ are the unit vectors along the x and y directions, respectively), to study the possible lattice rotational symmetry breaking.

III. NUMERICAL RESULTS

A. iPEPS results

We start by comparing the ground-state energy obtained by the iPEPS and finite-size DMRG calculations as shown in Figs. 2(a) and 2(b). The benchmark results agree quite well at the highly frustrated point $J_2 = 0.5$: the extrapolated values from a polynomial fit reveal that $E_{\mathrm{iPEPS}}^{D\to\infty} \simeq -1.507$ and $E_{\mathrm{DMRG}}^{L_y\to\infty} \simeq -1.506$. We find that the best-fitting curves for the DMRG and the iPEPS energy are obtained by the function $f(x) = a + \frac{b}{x^2} + \frac{c}{X^4}$, where $x = \frac{1}{D}$ and $\frac{1}{L_y}$. With growing J_2, we observe that the energy monotonically increases to $J_2 \sim 0.55$ through a sharp peak and then it starts to decrease, which may suggest a first-order quantum phase transition.

In Figs. 2(c) and 2(d), we present the iPEPS results of the order parameters $\{m, \Delta T_x, \Delta T_{x-y}\}$ to identify the nature of the ground state at $J_2 = 0.5$ and 0.6—since ΔT_y behaves similar to ΔT_x in our results, we only show the latter. For $J_2 = 0.5$, we obtain a finite value of $m \sim 0.48$ in the large-D limit, and its configuration is compatible with an AFM Néel state (see the inset, the graphical figure). The order parameters $\Delta T_x, \Delta T_{x-y}$ are strongly suppressed by increasing D, which agrees with a Néel state. The Néel state is strongly established at this point: even if we initialize the iPEPS with a random state or a stripe state, the outcome of the iPEPS simulation always gives a Néel state. Similarly, a stripe AFM state is established at $J_2 = 0.6$ as observed by the pattern of the local magnetic order [see the inset in Fig. 2(d)], the nonzero $\Delta T_{x-y} \simeq 0.2$, and the vanished ΔT_x. Therefore, we establish the Néel phase and the stripe phase on the small and large J_2 sides, respectively.

Next, we focus on the intermediate regime for $J_2 \sim 0.5$-0.6. We use the hysteresis analysis [61] (see Ref. [43]) to study

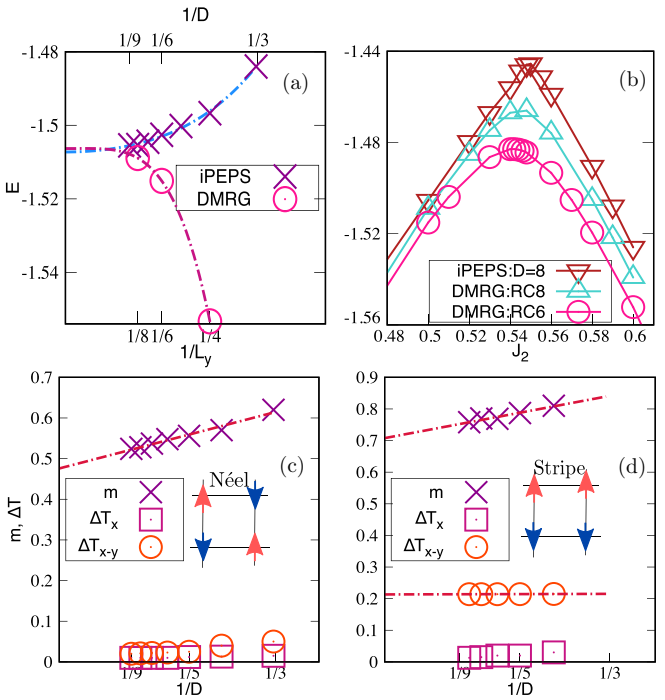

FIG. 2. Comparing the ground-state energy obtained by iPEPS and DMRG calculations. (a) The ground-state energy as a function of $1/D$ ($1/L_y$) at $J_2 = 0.5$ for iPEPS (DMRG). The DMRG data are for $L_y = 4$, 6, and 8. The dashed lines represent polynomial fits up to the fourth order. (b) The ground-state energy as a function of J_2. The sharp peak around $J_2 \sim 0.55$ suggests a first-order quantum phase transition. The order parameters $\{m, \Delta T_x, \Delta T_{x-y}\}$ as a function of $1/D$ for (c) $J_2 = 0.5$ and (d) $J_2 = 0.6$. They are respectively compatible with a Néel order and a stripe AFM order. The insets (graphical figures) show the pattern of the magnetization.

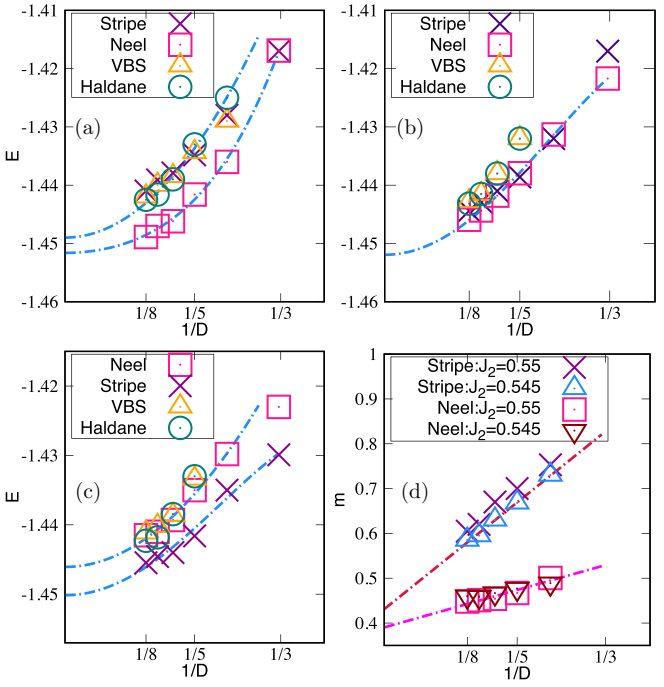

FIG. 3. A hysteresis analysis. Panels (a)–(c) are the iPEPS ground-state energy initialized using the different states of Néel, stripe, VBS, and Haldane at $J_2 = 0.545$, 0.548, and 0.55. (d) The magnetic order parameter m for $J_2 = 0.545$ and 0.55. A nonzero magnetic order parameter in the large-D limit implies a first-order quantum phase transition. In the stripe (Néel) phase, due to the hysteresis effect, the order parameter m with a Néel (stripe) pattern remains metastable.

phase transitions in this regime. The main idea is to initialize the iPEPS with different possible states and find whether the energies cross each other. The crossing of energy is considered as evidence of a quantum phase transition. Particularly, if in the vicinity of this crossing the order parameters (strongly) remain nonzero, this indicates a first-order phase transition. In addition to the Néel and stripe states, we also use the columnar VBS state and the Haldane state—both of them could be competitive candidates for a paramagnetic intermediate phase [20,62]. The Haldane state can be obtained by simply setting $J_2 = 0$ and $J_{1y} = 0$ (the nearest-neighbor coupling along the y direction), which results in a set of decoupled 1D Haldane chains. The nonmagnetic intermediate phase found in the previous DMRG calculation was proposed to be continuously connected to the Haldane phase [37]. The columnar VBS state consists of staggered singlet bonds (connecting all two adjacent spins) along either the x direction or the y direction.

In Figs. 3(a)–3(c), we have plotted the iPEPS ground-state energy initialized with different states at $J_2 = 0.545, 0.548$, and 0.55. For $J_2 = 0.545$, the Néel state gives the lowest energy. By increasing J_2, the energies get closer, and at $J_2 = 0.548$, it is found that the Néel and stripe states have almost the same energy—the Néel state still has slightly lower energy in the large-D limit. Finally, at $J_2 = 0.55$, the energy of the stripe state obviously becomes the lowest one. Our iPEPS results show that the energies of the Néel and stripe states cross each other at $J_2 \sim 0.549$. In this region, the energy of the Haldane state is always lower than the columnar VBS in the large-D limit; however, the columnar VBS state and the Haldane state never have energy lower than that of the magnetically ordered states.

We study the magnetic order parameter m to investigate the type of the quantum phase transition where the energies cross. As shown in Fig. 3(d), m shows the linear decreasing as a function of $1/D$: we obtain quite large values of the magnetization in the region $J_2 \sim 0.545$-0.55. For both $J_2 = 0.545$ and 0.55, the Néel and the stripe orders show $m = 0.39$ and 0.43 in the $D \to \infty$ limit. The nonzero magnetization through the quantum phase transition implies a first-order transition. Note that, due to the hysteresis effect, in the vicinity of a first-order quantum phase transition, the order parameter m with a Néel (stripe) pattern remains nonzero even in the stripe (Néel) phase [61].

Furthermore, we study the correlation function as another probe to investigate the quantum phase transition. In Fig. 4(a), we demonstrate the log-log plot of the spin-spin correlation function $C(r)$ at $J_2 = 0.548$ for different values of bond dimension D. It seems that $C(r)$ would have an exponential falloff, as it weakly depends on the bond dimension D. To get more insight, we compare the behavior of the correlation length at $J_2 = 0.549$, very close to the transition point, with the one deep inside the Néel phase (at the point $J_2 = 0.50$). For a

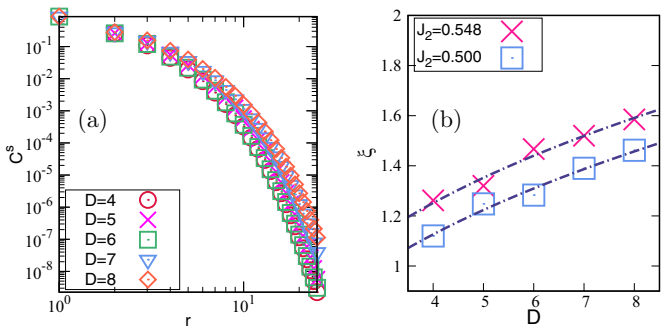

FIG. 4. Spin correlation function close to the quantum phase transition point. (a) Log-log plot of the spin-spin correlation function versus the site distance r. (b) The correlation lengths as a function of the bond dimension D for $J_2 = 0.5$ and 0.548. The dashed lines are power-law fits $\xi^s \sim D^\alpha$.

continuous quantum phase transition, one expects ξ^s to sharply grow as the system gets close to the critical point. We plot ξ^s as a function of the bond dimension D for $J_2 = 0.50$ and 0.549 in Fig. 4(b). The correlation length illustrates almost the same behavior: it similarly grows as $\xi^s \sim D^{0.35}$, which seems not to support a divergent correlation length at the transition point but could be consistent with a first-order transition.

B. DMRG results

Next, we demonstrate our DMRG results on the finite-L_y cylinder system. First of all, we show the magnetic order parameters $m^2(\pi,\pi)$ and $m^2(0,\pi)$ with L_y from 4 to 10 in Figs. 5(a) and 5(b). Through appropriate finite-size scaling, we find that the Néel order $m^2(\pi,\pi)$ could persist to $J_2 \simeq 0.545$. For $J_2 > 0.55$, the stripe order $m^2(0,\pi)$ develops very fast with growing J_2, as shown by $J_2 = 0.552$ in Fig. 5(b). Compared with the previous DMRG results based on the size scaling up to the $L_y = 8$ torus [37], our analysis up to the $L_y = 10$ cylinder suggests a much smaller regime, $0.545 < J_2 < 0.55$, for a possible intermediate phase. The log-log plots of m^2 versus L_y in Figs. 5(c) and 5(d) also agree with the transition between different orders at $J_2 \simeq 0.55$, where the two magnetic orders change their behaviors dramatically. At $J_2 = 0.55$, both magnetic order parameters seem to follow a critical behavior. Such a critical-like behavior of order parameters could be consistent with a continuous phase transition at $J_2 \simeq 0.55$. Here, we remark that the system size in our DMRG calculation is too small for such a critical analysis. And previous studies [36] and our results have already shown that the transition at $J_2 \simeq 0.55$ is a first-order transition.

Since the different orders may break different lattice symmetries, here we study the lattice order by calculating the nearest-neighbor bond energy $\langle \mathbf{S}_i \cdot \mathbf{S}_j \rangle$. In Fig. 6(a), we show the nearest-neighbor J_1 bond energy for $J_2 = 0.548$ on the RC8-16 cylinder, which is in the possible intermediate regime. We can see that although the open boundaries of the cylinder break lattice translational symmetry along the x direction, the bond energy in the bulk of the cylinder is quite uniform. We also find that the bond energy difference on the open edges decays quite fast to the uniform bulk value (not shown here), indicating a very small boundary effect. Thus, the

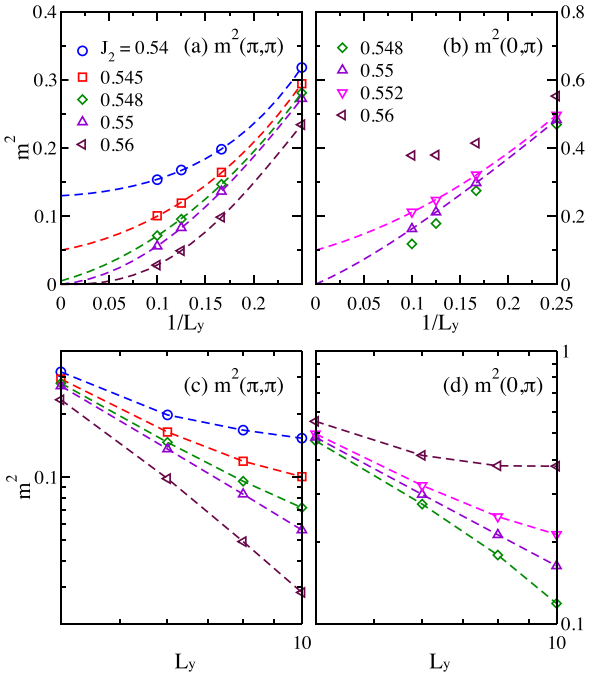

FIG. 5. Finite-size scaling of magnetic order parameters on the RCL_y-2L_y cylinders with $L_y = 4$, 6, 8, and 10. Panels (a) and (b) show the Néel and the stripe order parameters $m^2(\pi,\pi)$ and $m^2(0,\pi)$ versus $1/L_y$, respectively. The dashed lines are the polynomial fits up to the fourth order. Panels (c) and (d) show the corresponding log-log plots versus L_y, where the dashed lines are guides to the eye.

lattice translational symmetry is preserved in the intermediate regime, which is different from the DMRG results of the spin-1 J_1-J_2 honeycomb model, in which the system shows a strong tendency to form a plaquette VBS in the intermediate phase [63].

Although the bond energy for $J_2 = 0.548$ in Fig. 6(a) preserves the translational symmetry, it shows a strong bond nematicity. To investigate the possibility of the lattice rotational symmetry breaking, we study the bond nematic order σ_1, which is defined as $\sigma_1 = \langle \mathbf{S}_i \cdot \mathbf{S}_{i+\hat{x}} \rangle - \langle \mathbf{S}_i \cdot \mathbf{S}_{i+\hat{y}} \rangle$. For the Néel phase with $\mathbf{q} = (\pi,\pi)$, σ_1 should be vanished; on the other hand, it should be finite in the stripe phase with $\mathbf{q} = (0,\pi)/(\pi,0)$. In Fig. 6(b), we show the finite-size scaling of σ_1 versus $1/L_y$. We should emphasize that although the cylinder geometry has already broken the lattice C_4 rotational symmetry, the size scaling has been shown, in different phases, to be an effective way to determine whether the nematic order would be finite or not in the large-size limit [30,31]. In the inset, we present the nematic order σ_1 versus different lengths L_x with fixed L_y. We find that σ_1 is almost invariant with growing L_x, which indicates small finite-size effects along the x direction. Although the results shown in the inset are only for $J_2 = 0.548$, it holds for general J_2. For $J_2 \lesssim 0.545$, σ_1 decays fast and tends to vanish in the thermodynamic limit, which is consistent with the Néel phase. For $J_2 \geqslant 0.55$, σ_1 goes to a finite value with increasing L_y, which agrees with the stripe-order breaking lattice C_4 symmetry. In a small intermediate regime such as $J_2 = 0.548$, σ_1 decreases with growing cylinder width; however, because of the system size limit, our DMRG results

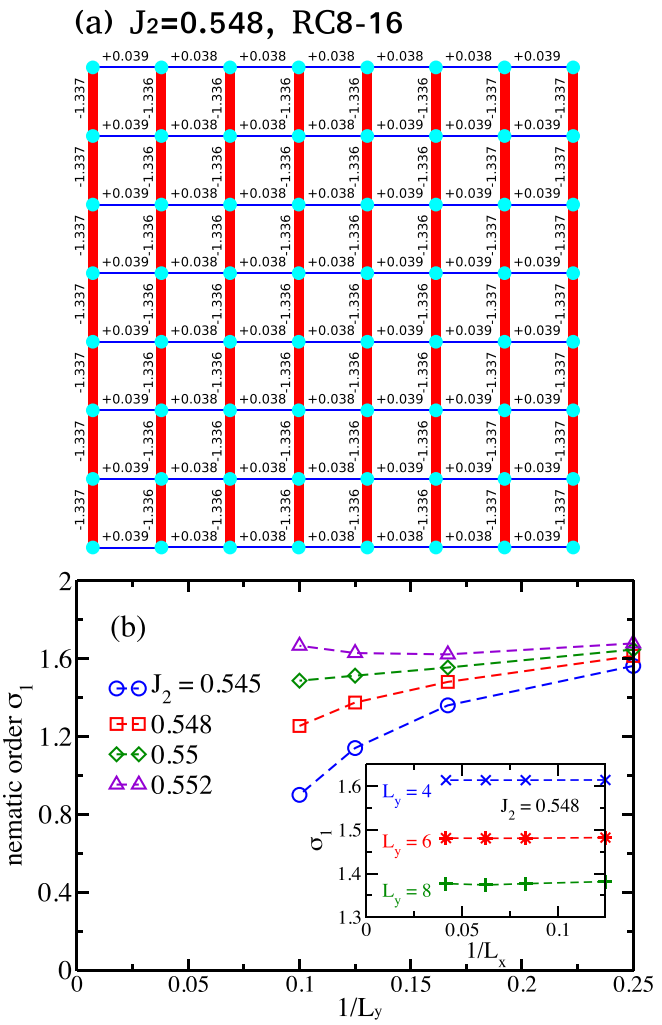

FIG. 6. Lattice orders in the intermediate regime. (a) Nearest-neighbor J_1 bond energy for $J_2 = 0.548$ on the RC8-16 cylinder. Here we show the middle 8×8 sites. The numbers denote the J_1 bond energy $\langle \mathbf{S}_i \cdot \mathbf{S}_j \rangle$. (b) Finite-size scaling of the lattice nematic order parameter σ_1 for different J_2 couplings. The inset shows the weak dependence of σ_1 on the cylinder length L_x.

cannot determine the nematic order in the thermodynamic limit.

We also calculate the spin triplet gap of the system. The triplet gap is defined as $\Delta E = E_1 - E_0$, where E_1 is the lowest-energy state in the total spin $S = 1$ sector and E_0 is the ground-state energy in the $S = 0$ sector. We calculate the gap by first obtaining the ground state on the RCL_y-2L_y cylinder and then sweeping the middle $L_y \times L_y$ sites in the total spin $S = 1$ sector, avoiding the open-edge excitations [64]. In Fig. 7(a), we demonstrate the triplet gap with growing J_2 on the RC4 and RC6 cylinders. The gap grows sharply near $J_2 \simeq 0.55$ on the finite-size systems, which seems to suggest a finite gap. Note that as the convergence challenge for targeting the $S = 1$ sector, we calculate the gap on the $L_y = 8$ cylinder for only a few J_2 points. In Fig. 7(b), we show the finite-size scaling of the gap for different J_2. For $J_2 = 0.2$ and 0.6, the quickly decreasing gap is consistent with the magnetic

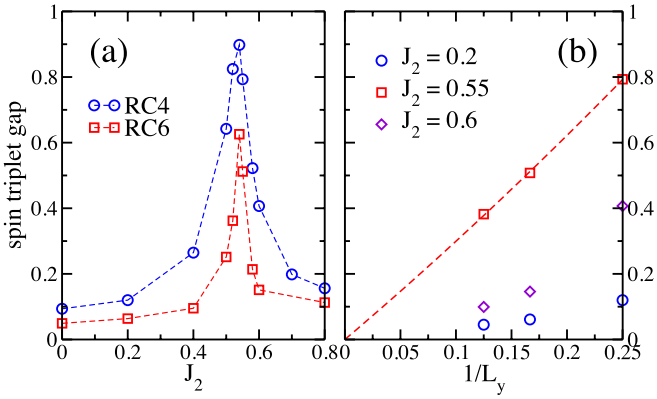

FIG. 7. Spin triplet gap on the finite-size systems. (a) The triplet gap versus J_2 on the $L_y = 4$ and 6 cylinders. (b) Finite-size scaling of the triplet gap versus $1/L_y$ in the different phases. The spin gap is obtained by sweeping the middle $L_y \times L_y$ sites in the spin-1 sector based on the ground state of the RCL_y-2L_y cylinder. For the data at $J_2 = 0.55$, the gap is fitted by using $1/L_y$ up to the second order.

orders spontaneously breaking the spin rotational symmetry. For $J_2 = 0.55$, the gap drops fast and seems to be consistent with vanishing in the large-size limit. In our DMRG calculation with the improved system size, the possible intermediate regime shrinks rapidly compared with the previous DMRG result [37], which suggests strong finite-size effects and may imply a direct phase transition between the two magnetic order phases that could be consistent with the vanished spin triplet gap.

IV. SUMMARY AND DISCUSSION

We have used the combined numerical methods of the iPEPS ansatz and the SU(2) DMRG to study the ground-state phase diagram of the spin-1 J_1-J_2 Heisenberg model on the square lattice. While the iPEPS ansatz probes the nature of the quantum phase directly in the thermodynamic limit, the DMRG calculation obtains accurate results on a cylinder system with finite L_y. The final data of the iPEPS and DMRG calculations are respectively obtained by using the finite-D and finite-L_y scaling.

In our iPEPS simulation, we find that the lowest-energy state transits from the Néel state to the stripe state directly at $J_2 \simeq 0.549$. Even if the iPEPS ansatz is biased toward the competitive paramagnetic states (Haldane and VBS), it could not provide energy lower than that of the magnetically ordered states. The correlation length near the transition appears to be finite in the large-D limit, supporting a first-order transition between the two magnetic order phases. In the finite-size DMRG calculation, our finite-size scaling analysis up to $L_y = 10$ finds that the previously proposed intermediate regime [37] shrinks rapidly with increasing L_y; as such a dramatic change implies the vanished intermediate phase. In our DMRG results, the stripe order grows up sharply at $J_2 \simeq 0.55$, also supporting a first-order transition consistent with the iPEPS result.

Our study opens up the door to reexamine the phase diagram of the spin-1 J_{1x}-J_{1y}-J_2 Heisenberg model on the square lattice, where J_{1x} and J_{1y} are the spacial anisotropic nearest-neighbor

interactions. While the Schwinger-Boson mean-field theory predicted a fluctuation-induced first-order transition between the Néel phase and the stripe phase, which only terminates at a tricritical point for a large anisotropy $(J_{1y} - J_{1x})/J_{1y}$, previous DMRG results suggested a nonmagnetic phase emerging near the transition line [37]. Our results have shown that the nonmagnetic phase in the isotropic case ($J_{1x} = J_{1y}$) is unlikely, thus it would be interesting to study whether the anisotropy could enhance quantum fluctuations and open a paramagnetic phase in the intermediate regime.

ACKNOWLEDGMENTS

The research was partly supported by National Science Foundation Grants PREM DMR-1205734 (R.H.), and by the start-up funding from Beihang University (S.S.G.). Work by DNS was supported by the Department of Energy, Office of Basic Energy Sciences, Division of Materials Sciences and Engineering, under Contract No. DE-AC02-76SF00515 through SLAC National Accelerator Laboratory. We have used Uni10 [65] as a middleware library to build the iPEPS ansatz.

[1] L. Balents, Spin liquids in frustrated magnets, Nature (London) **464**, 199 (2010).

[2] L. Savary and L. Balents, Quantum spin liquids: A review, Rep. Prog. Phys. **80**, 016502 (2016).

[3] I. Affleck, T. Kennedy, E. H. Lieb, and H. Tasaki, Rigorous Results on Valence-Bond Ground States in Antiferromagnets, Phys. Rev. Lett. **59**, 799 (1987).

[4] N. Read and S. Sachdev, Valence-Bond and Spin-Peierls Ground States of Low-Dimensional Quantum Antiferromagnets, Phys. Rev. Lett. **62**, 1694 (1989).

[5] N. Read and S. Sachdev, Spin-Peierls, valence-bond solid, and Néel ground states of low-dimensional quantum antiferromagnets, Phys. Rev. B **42**, 4568 (1990).

[6] P. W. Anderson, Resonating valence bonds: A new kind of insulator? Mater. Res. Bull. **8**, 153 (1973).

[7] X. G. Wen and Q. Niu, Ground-state degeneracy of the fractional quantum hall states in the presence of a random potential and on high-genus Riemann surfaces, Phys. Rev. B **41**, 9377 (1990).

[8] N. Read and S. Sachdev, Large-N Expansion for Frustrated Quantum Antiferromagnets, Phys. Rev. Lett. **66**, 1773 (1991).

[9] T. Senthil, A. Vishwanath, L. Balents, S. Sachdev, and M. P. A. Fisher, Deconfined quantum critical points, Science **303**, 1490 (2004).

[10] L. B. Ioffe and A. I. Larkin, Effective action of a two-dimensional antiferromagnetic, Int. J. Mod. Phys. B **02**, 203 (1988).

[11] M. E. Zhitomirsky and K. Ueda, Valence-bond crystal phase of a frustrated spin-1/2 square-lattice antiferromagnet, Phys. Rev. B **54**, 9007 (1996).

[12] J. H. Xu and C. S. Ting, Phase diagram of the frustrated square Heisenberg lattice based upon a modified spin-wave theory, Phys. Rev. B **42**, 6861 (1990).

[13] C. Bruder and F. Mila, Spin waves and stability of magnetic order in frustrated magnets, Europhys. Lett. **17**, 463 (1992).

[14] H.-C. Jiang, H. Yao, and L. Balents, Spin liquid ground state of the spin-$\frac{1}{2}$ square J_1-J_2 Heisenberg model, Phys. Rev. B **86**, 024424 (2012).

[15] W.-J. Hu, F. Becca, A. Parola, and S. Sorella, Direct evidence for a gapless Z_2 spin liquid by frustrating Néel antiferromagnetism, Phys. Rev. B **88**, 060402 (2013).

[16] L. Wang, D. Poilblanc, Z.-C. Gu, X.-G. Wen, and F. Verstraete, Constructing a Gapless Spin-Liquid State for the Spin-1/2J_1-J_2 Heisenberg Model on a Square Lattice, Phys. Rev. Lett. **111**, 037202 (2013).

[17] S.-S. Gong, W. Zhu, D. N. Sheng, O. I. Motrunich, and M. P. A. Fisher, Plaquette Ordered Phase and Quantum Phase Diagram in the Spin-$\frac{1}{2}$ J_1-J_2 Square Heisenberg Model, Phys. Rev. Lett. **113**, 027201 (2014).

[18] S. Morita, R. Kaneko, and M. Imada, Quantum spin liquid in spin 1/2 j_1-j_2 Heisenberg model on square lattice: Many-variable variational Monte Carlo study combined with quantum-number projections, J. Phys. Soc. Jpn. **84**, 024720 (2015).

[19] L. Wang and A. W. Sandvik, Critical level crossings in the square-lattice spin-1/2 J_1-J_2 Heisenberg antiferromagnet, arXiv:1702.08197.

[20] R. Haghshenas and D. N. Sheng, $U(1)$-symmetric infinite projected entangled-pair states study of the spin-1/2 square J_1-J_2 Heisenberg model, Phys. Rev. B **97**, 174408 (2018).

[21] C. Xu, M. Müller, and S. Sachdev, Ising and spin orders in the iron-based superconductors, Phys. Rev. B **78**, 020501 (2008).

[22] Q. Si and E. Abrahams, Strong Correlations and Magnetic Frustration in the High T_c Iron Pnictides, Phys. Rev. Lett. **101**, 076401 (2008).

[23] C. Fang, H. Yao, W.-F. Tsai, J.P. Hu, and S. A. Kivelson, Theory of electron nematic order in lafeaso, Phys. Rev. B **77**, 224509 (2008).

[24] J. K. Glasbrenner, J. P. Velev, and I. I. Mazin, First-principles study of the minimal model of magnetic interactions in Fe-based superconductors, Phys. Rev. B **89**, 064509 (2014).

[25] R. Yu and Q. Si, Antiferroquadrupolar and Ising-Nematic Orders of a Frustrated Bilinear-Biquadratic Heisenberg Model and Implications for the Magnetism of FeSe, Phys. Rev. Lett. **115**, 116401 (2015).

[26] F. Wang, S. A Kivelson, and D.-H. Lee, Nematicity and quantum paramagnetism in FeSe, Nat. Phys. **11**, 959 (2015).

[27] H.-H. Lai, W.-J. Hu, R. Yu, and Q. Si, Antiferroquadrupolar Order and Rotational Symmetry Breaking in a Generalized Bilinear-Biquadratic Model on a Square Lattice, Phys. Rev. Lett. **118**, 176401 (2017).

[28] Z. Wang, W.-J. Hu, and A. H. Nevidomskyy, Spin Ferroquadrupolar Order in the Nematic Phase of FeSe, Phys. Rev. Lett. **116**, 247203 (2016).

[29] H.-F. Zhu, H.-Y. Cao, Y. Xie, Y.-S. Hou, S. Chen, H. Xiang, and X.-G. Gong, Giant biquadratic interaction-induced magnetic anisotropy in the iron-based superconductor $A_x Fe_{2-y} Se_2$, Phys. Rev. B **93**, 024511 (2016).

[30] W.-J. Hu, H.-H. Lai, S.-S. Gong, R. Yu, A. H. Nevidomskyy, and Q. Si, Frustrated magnetism and quantum transitions of nematic phases in FeSe, arXiv:1606.01235.

[31] S.-S. Gong, W. Zhu, D. N. Sheng, and K. Yang, Possible nematic spin liquid in spin-1 antiferromagnetic system on the square lattice: Implications for the nematic paramagnetic state of FeSe, Phys. Rev. B **95**, 205132 (2017).

[32] I. Niesen and P. Corboz, Emergent Haldane phase in the $S = 1$ bilinear-biquadratic Heisenberg model on the square lattice, Phys. Rev. B **95**, 180404 (2017).

[33] W.-J. Hu, S.-S. Gong, H.-H. Lai, H. Hu, Q. Si, and A. H. Nevidomskyy, Nematic liquid phase in a frustrated spin-1 system on the square lattice, arXiv:1711.06523.

[34] I. G. Gochev, Spin-wave interaction effects in the Néel phase of the J_1-J_2-J_3 model, Phys. Rev. B **51**, 16421 (1995).

[35] F. Mila, D. Poilblanc, and C. Bruder, Spin dynamics in a frustrated magnet with short-range order, Phys. Rev. B **43**, 7891 (1991).

[36] R. F. Bishop, P. H. Y. Li, R. Darradi, and J. Richter, The quantum J_1-J'_1-J_2 spin-1/2 Heisenberg model: Influence of the interchain coupling on the ground-state magnetic ordering in two dimensions, J. Phys.: Condens. Matter **20**, 255251 (2008).

[37] H. C. Jiang, F. Krüger, J. E. Moore, D. N. Sheng, J. Zaanen, and Z. Y. Weng, Phase diagram of the frustrated spatially-anisotropic $S = 1$ antiferromagnet on a square lattice, Phys. Rev. B **79**, 174409 (2009).

[38] F. D. M. Haldane, Nonlinear Field Theory of Large-Spin Heisenberg Antiferromagnets: Semiclassically Quantized Solitons of the One-Dimensional Easy-Axis Néel State, Phys. Rev. Lett. **50**, 1153 (1983).

[39] There is a similar study of the same spin-1 J_1-J_2 square Heisenberg model by J.-Y. Chen, S. Capponi, and D. Poilblanc (private communication).

[40] J. Jordan, R. Orús, G. Vidal, F. Verstraete, and J. I. Cirac, Classical Simulation of Infinite-Size Quantum Lattice Systems in Two Spatial Dimensions, Phys. Rev. Lett. **101**, 250602 (2008).

[41] V. Murg, F. Verstraete, and J. I. Cirac, Exploring frustrated spin systems using projected entangled pair states, Phys. Rev. B **79**, 195119 (2009).

[42] S. Singh, R. N. C. Pfeifer, and G. Vidal, Tensor network decompositions in the presence of a global symmetry, Phys. Rev. A **82**, 050301 (2010).

[43] P. Corboz and F. Mila, Tensor network study of the Shastry-Sutherland model in zero magnetic field, Phys. Rev. B **87**, 115144 (2013).

[44] F. Verstraete, V. Murg, and J. I. Cirac, Matrix product states, projected entangled pair states, and variational renormalization group methods for quantum spin systems, Adv. Phys. **57**, 143 (2008).

[45] J. Eisert, Entanglement and tensor network states, arXiv:1308.3318.

[46] B. Bauer, P. Corboz, R. Orús, and M. Troyer, Implementing global Abelian symmetries in projected entangled-pair state algorithms, Phys. Rev. B **83**, 125106 (2011).

[47] P. Corboz, J. Jordan, and G. Vidal, Simulation of fermionic lattice models in two dimensions with projected entangled-pair states: Next-nearest neighbor Hamiltonians, Phys. Rev. B **82**, 245119 (2010).

[48] M. Suzuki, Fractal decomposition of exponential operators with applications to many-body theories and Monte Carlo simulations, Phys. Lett. A **146**, 319 (1990).

[49] H. N. Phien, J. A. Bengua, H. D. Tuan, P. Corboz, and R. Orús, Infinite projected entangled pair states algorithm improved: Fast full update and gauge fixing, Phys. Rev. B **92**, 035142 (2015).

[50] H. C. Jiang, Z. Y. Weng, and T. Xiang, Accurate Determination of Tensor Network State of Quantum Lattice Models in Two Dimensions, Phys. Rev. Lett. **101**, 090603 (2008).

[51] Z.-C. Gu, M. Levin, and X.-G. Wen, Tensor-entanglement renormalization group approach as a unified method for symmetry breaking and topological phase transitions, Phys. Rev. B **78**, 205116 (2008).

[52] P. Corboz, R. Orús, B. Bauer, and G. Vidal, Simulation of strongly correlated fermions in two spatial dimensions with fermionic projected entangled-pair states, Phys. Rev. B **81**, 165104 (2010).

[53] T. Nishino and K. Okunishi, Corner transfer matrix algorithm for classical renormalization group, J. Phys. Soc. Jpn. **66**, 3040 (1997).

[54] P. Corboz, T. M. Rice, and M. Troyer, Competing States in the t-J Model: Uniform d-Wave State Versus Stripe State, Phys. Rev. Lett. **113**, 046402 (2014).

[55] Y.-K. Huang, P. Chen, and Y.-J. Kao, Accurate computation of low-temperature thermodynamics for quantum spin chains, Phys. Rev. B **86**, 235102 (2012).

[56] M. Matsumoto, C. Yasuda, S. Todo, and H. Takayama, Ground-state phase diagram of quantum Heisenberg antiferromagnets on the anisotropic dimerized square lattice, Phys. Rev. B **65**, 014407 (2001).

[57] G. Evenbly and G. Vidal, Tensor network states and geometry, J. Stat. Phys. **145**, 891 (2011).

[58] F. Verstraete, M. M. Wolf, D. Perez-Garcia, and J. I. Cirac, Criticality, the Area Law, and the Computational Power of Projected Entangled Pair States, Phys. Rev. Lett. **96**, 220601 (2006).

[59] S. R. White, Density Matrix Formulation for Quantum Renormalization Groups, Phys. Rev. Lett. **69**, 2863 (1992).

[60] I. P McCulloch and M. Gulácsi, The non-Abelian density matrix renormalization group algorithm, Europhys. Lett. **57**, 852 (2002).

[61] In the case of a Néel-to-stripe first-order phase transition, the order states directly cross each other, because at the critical point both equally exist. One expects that slightly above the critical point, in the stripe phase, the Néel state would be a pseudo ground state: a finite-D iPEPS ansatz initialized by the Néel state probably fails to converge to the stripe state. This effect as the order states remain metastable around the critical point is referred to as a hysteresis effect.

[62] M. Sadrzadeh, R. Haghshenas, S. S. Jahromi, and A. Langari, Emergence of string valence-bond-solid state in the frustrated J_1-J_2 transverse field Ising model on the square lattice, Phys. Rev. B **94**, 214419 (2016).

[63] S.-S. Gong, W. Zhu, and D. N. Sheng, Quantum phase diagram of the spin-1 J_1-J_2 Heisenberg model on the honeycomb lattice, Phys. Rev. B **92**, 195110 (2015).

[64] S. Yan, D. A. Huse, and S. R. White, Spin-liquid ground state of the S = 1/2 kagome Heisenberg antiferromagnet, Science **332**, 1173 (2011).

[65] Y.-J. Kao, Y.-D. Hsieh, and P. Chen, Uni10: An open-source library for tensor network algorithms, J. Phys.: Conf. Ser. **640**, 012040 (2015).